remote sensing

MDPI

Article

Downscaling of Surface Soil Moisture Retrieval by Combining MODIS/Landsat and In Situ Measurements

Chenyang Xu [1,*], John J. Qu [1], Xianjun Hao [1], Michael H. Cosh [2], John H. Prueger [3], Zhiliang Zhu [4] and Laurel Gutenberg [1]

1 Global Environment and Natural Resources Institute (GENRI) and Department of Geography and GeoInformation Science (GGS), College of Science, George Mason University, Fairfax, VA 22032, USA; jqu@gmu.edu (J.J.Q.); xhao1@gmu.edu (X.H.); laurelgutenberg@gmail.com (L.G.)
2 Hydrology and Remote Sensing Laboratory of USDA ARS, Beltsville, MD 20705, USA; michael.cosh@ars.usda.gov
3 USDA ARS National Soil Tilth Laboratory, Ames, IA 50011, USA; John.Prueger@ars.usda.gov
4 U.S. Geological Survey, Reston, VA 20192, USA; zzhu@usgs.gov
* Correspondence: cxu8@masonlive.gmu.edu; Tel.: +1-703-993-4012

Received: 28 November 2017; Accepted: 29 January 2018; Published: 1 Febuary 2018

Abstract: Soil moisture, especially surface soil moisture (SSM), plays an important role in the development of various natural hazards that result from extreme weather events such as drought, flooding, and landslides. There have been many remote sensing methods for soil moisture retrieval based on microwave or optical thermal infrared (TIR) measurements. TIR remote sensing has been popular for SSM retrieval due to its fine spatial and temporal resolutions. However, because of limitations in the penetration of optical TIR radiation and cloud cover, TIR methods can only be used under clear sky conditions. Microwave SSM retrieval is based on solid physical principles, and has advantages in cases of cloud cover, but it has low spatial resolution. For applications at the local scale, SSM data at high spatial and temporal resolutions are important, especially for agricultural management and decision support systems. Current remote sensing measurements usually have either a high spatial resolution or a high temporal resolution, but not both. This study aims to retrieve SSM at both high spatial and temporal resolutions through the fusion of Moderate Resolution Imaging Spectroradiometer (MODIS) and Land Remote Sensing Satellite (Landsat) data. Based on the universal triangle trapezoid, this study investigated the relationship between land surface temperature (LST) and the normalized difference vegetation index (NDVI) under different soil moisture conditions to construct an improved nonlinear model for SSM retrieval with LST and NDVI. A case study was conducted in Iowa, in the United States (USA) (Lat: 42.2°~42.7°, Lon: −93.6°~−93.2°), from 1 May 2016 to 31 August 2016. Daily SSM in an agricultural area during the crop-growing season was downscaled to 120-m spatial resolution by fusing Landsat 8 with MODIS, with an R^2 of 0.5766, and RMSE from 0.0302 to 0.1124 m^3/m^3.

Keywords: surface soil moisture; downscaling; data fusion; universal triangle method; land surface temperature; fractional vegetation coverage; cross sensor; in situ measurements

1. Introduction

Soil moisture is an important element of the global environment and land surface system, and plays an essential role in the crop growing season. It is one of the most important parameters for evaluating potential agricultural drought conditions [1–3]. There is growing recognition of the importance of soil moisture in the environmental cycle, with the surface layer acting as an interface

between the land and the atmosphere. Surface soil moisture (SSM) has a crucial impact on the exchange of water and heat energy between the atmosphere and the land surface through transpiration or evaporation [4–7]. It is of great importance to many other environmental and economic issues that are related to drought, flooding, and water and food security [8–10]. SSM also plays an important role in feedback mechanisms for the development of weather systems affecting precipitation patterns. Moreover, SSM is an important parameter in the land surface model, closely linking the water vapor in the atmosphere, surface water, and groundwater in the study of the entire ecological system [4,11,12].

In situ measurements are the most reliable way for monitoring soil moisture in both the surface layer and sub-surface layers at various depths. However, these measurements are point-source data that generally have limited spatial and temporal coverage. Remote sensing methods offer the best means of SSM estimation at a large spatial extent. At present, SSM can be retrieved by a variety of remote sensing techniques. Microwave technology has demonstrated a quantitative ability to estimate soil moisture physically for a wide range of vegetation cover. The Soil Moisture and Ocean Salinity (SMOS) mission [13] and The Soil Moisture Active Passive (SMAP) mission [14] are two of the most recent satellite missions for global soil moisture retrieval using microwave remote sensing. However, the spatial resolutions of current satellite microwave radiometers are not optimal for land remote sensing, especially SSM monitoring. This is due to practical problems related to supporting a large, low-frequency antenna in space. Methods with optical thermal infrared (TIR) remote sensing measurements from Terra/Aqua Moderate Resolution Imaging Spectroradiometer (MODIS) and Land Remote Sensing (Landsat) Thematic Mapper (TM)/Enhanced Thematic Mapper (ETM)/Thermal Infrared Sensor (TIRS) data have been used for SSM monitoring at moderate or high spatial resolutions based on the universal triangular relationship between land surface temperature (LST) and the normalized difference vegetation index (NDVI) [15,16].

Some research works have been conducted that fuse Landsat data with MODIS measurements, such as the Spatial and Temporal Adaptive Reflectance Fusion Model (STARFM) [17], the Spatio-temporal Adaptive Data Fusion Algorithm for Temperature mapping (SADFAT) [18], the Spatio-temporal image fusion model (STI-FM) [19], and so on. Dr. Feng Gao proposed the first data fusion method STARFM [17], which aimed to generate solar reflective bands at fine spatial and temporal resolutions by fusing MODIS and Landsat measurements. Some other methods have been developed since that have been based on STARFM for thermal emissive band fusion to retrieve LST at high spatial resolution, such as SADFAT [18]. However, there is no existing method for the fusion of both solar reflective bands and thermal emissive bands. For SSM monitoring at high spatial and temporal resolutions, it is necessary to fuse both the solar reflective and thermal emissive measurements with consistent methods. After analyzing the merits and limitations of many existed fusion models [20–23], it was found that if the solar reflective bands and thermal emissive bands are fused separately through different approaches, there may be bias, because of the inconsistency between different fusion methods.

Focusing on the challenge of SSM monitoring at both high spatial and temporal resolutions, this study proposes a new SSM estimation approach with data fusion techniques. Landsat 8 datasets are fused with MODIS datasets at similar channels with both datasets to improve the spatial and temporal resolutions. As a result, the influence of weather conditions can be reduced, and the integration of these datasets with ground in situ measurements can be enhanced. The primary objective of this study is to downscale SSM through thermal remote sensing methods during the crop growing season in an agricultural area. Both solar reflective and thermal emissive bands are fused in this study in order to calculate LST and NDVI values, which will be used further in the universal triangle method to retrieve SSM at 120 m spatial resolution. The results of the predicted LST were validated with MODIS and Landsat 8 LST products. An analysis of soil moisture data at 120 m resolution over the study area showed details of spatial variation and temporal change, and demonstrated good potential for agricultural applications at the local scale.

2. Study Area and Data

2.1. Study Area

The study area is located in Iowa, on the central and northern plain of the United States (U.S.). The United States Department of Agriculture Agricultural Research Services (USDA-ARS) maintains the South Fork Experimental Watershed, which ranges from 42.2° N to 42.7° N, 93.6° W to 93.2° W, and covers an area of approximately 60 million hectares, with the elevation ranges from 1250 m to 1585 m MSL. The climate is humid, with an annual average rainfall of 835 mm. May and June have the heaviest precipitation. An intensive field experiment, the Soil Moisture Active Passive Validation Experiment (SMAPVEX16), was conducted in 2016, during May, June, July, and August; this study will focus on the time period 1 May to 31 August 2016. The study area was one of the major grain production areas in the U.S. Corn and soybean are the primary crops in this area, and the soil is dominated by loams and silty clay loams.

Figure 1a shows the location of the study area in Iowa; Figure 1b shows the locations of the permanent and temporary sites in the study area.

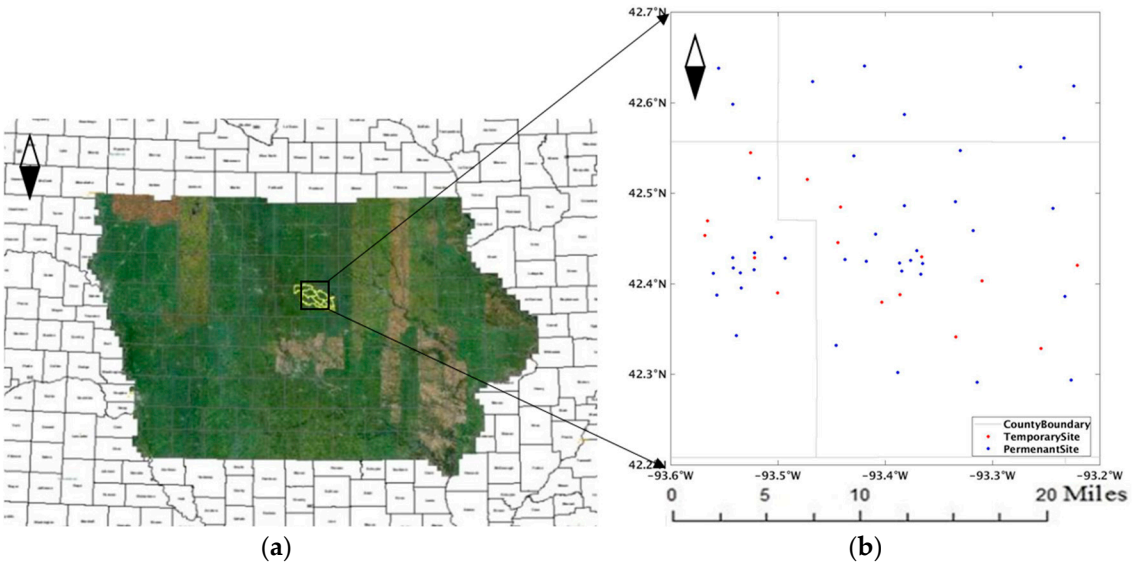

Figure 1. (**a**) Location of South Fork Experimental Watershed (from Michael H. Cosh); (**b**) the locations of permanent (red) and temporary (blue) sites in the study area.

Table 1 is the crop types of the 15 permanent sites that were used in this study to validate the retrieved SSM results.

Table 1. Crop type for permanent sites.

Crop Type	Site
Corn	SF01, SF02, SF04, SF09, SF10, SF13, SF15
Soybean	SF03, SF05, SF06, SF07, SF14
Corn and Soybean	SF08, SF11, SF12

2.2. Data

2.2.1. Remote Sensing Datasets

This study used Landsat 8 and MODIS datasets for SSM downscaling. Landsat 8 carries an Operation Land Imager (OLI) and a TIRS, and can collect global 30-m spatial resolution multispectral

images with a 16-day recycle period. The TIRS has two thermal infrared bands, which is an improvement compared with the former Landsat satellite series. Reflectance band 4, reflectance band 5, and the thermal band TIR2 were chosen from Landsat 8 to calculate the NDVI and LST, which were used further for SSM retrieval. The study area was covered by two Landsat pixels: row 28/column 30 and row 27/column 30. Since most observation days for row 27/col 30 are too cloudy to collect enough useful information, the pixel of row 28/col 30 was chosen instead.

MODIS is onboard both the Terra and Aqua satellites. MODIS has measurements in 36 spectral bands and global coverage in 1–2 day products; MOD02, MOD05, and MOD11 were chosen for this study. MOD02 is the MODIS level 1B product (solar reflective bands 1 and 2 and thermal infrared band 32, which provides the calibrated Earth View). MOD05 is the MODIS level 2 atmospheric precipitable water products; it was used to get a cloud mask to exclude the cloud area in the study area, and collect the water vapor content in the atmosphere. MOD11 is the MODIS land surface temperature and emissivity product, which was used to validate the accuracy of the LST from data fusion.

Landsat TIR2 and MODIS band 32 were used for the thermal infrared band fusion. Landsat 8 band 4 and MODIS band 1 were used for the near-infrared band fusion, while Landsat 8 band 5 and MODIS band 2 were used for the red band fusion. The fused near-infrared reflectance data, and red reflectance data were used to calculate the NDVI for further use. Table 2 are the MODIS bands and Landsat 8 bands that were used in this study.

Table 2. Moderate Resolution Imaging Spectroradiometer (MODIS) (1000 m) and Land Remote Sensing Satellite (Landsat 8) (30 m) corresponding bands.

MODIS		Landsat 8	
Band 1	Band 1, 620 nm to 670 nm, is primarily used for land, cloud, and aerosols boundaries.	Band 4	Band 4, 636 nm to 673 nm, is a red band.
Band 2	Band 2, 841 nm to 876 nm, is primarily used for land, cloud, and aerosols properties.	Band 5	Band 5, 851 nm to 879 nm, is a near infrared band.
Band 32	Band 32, 11.77 um to 12.27 um, is primarily used for surface and cloud temperature.	TIR2	TIR2, 11.50 um to 12.51 um, is a thermal infrared band.

2.2.2. In Situ Measurements

In situ measurements in this study were collected during the Soil Moisture Active Passive Validation Experiment 2016—Iowa (SMAPVEX16-IA). The temporary and permanent sites collected hourly soil moisture at 5-cm depth during the study period using a Stevens Water Hydra Probe (Stevens Water Monitoring Systems, Portland, OR, USA) Gravimetrically, USDA-ARS collected the soil moisture values during an extensive field campaign to validate and calibrate the soil moisture monitoring network.

There are two intensive observing periods (IOPs) from May to August. The aircraft that carried the Passive/Active L-Band Sensor (PALS) was used to collect ground measurements of soil moisture, soil temperature, and soil roughness combined with ground sampling. All of the parameters measured during the campaign were used to calibrate and validate the measurements from the permanent and temporary sites. There are mainly three parts for the ground soil moisture sampling: temporary in situ stations, remote COsmic-ray Soil Moisture Observing System (COSMOS) rover technology, and high-density gravimetric sampling. The major goal of the ground sampling is to improve the scaling functions for the core validation sites (CVS) and the quality of the in-situ sensor estimation, and provide soil moisture products with high resolution over the study area.

There are 15 sites with hydra probes installed at 5 cm, 10 cm, 20 cm, and 50 cm by the USDA-ARS to monitor soil conditions at different depths. Soil moisture measured at 5 cm depth was chosen in this

study. An additional 40 temporal hydra probes were installed during the crop-growing seasons to monitor the soil moisture and soil temperature at the same depths. Fieldwork was done during 25 May to 5 June and 3 August to 16 August 2016; these manual measurements were used for the recalibration and validation of the soil probe measurements in the permanent and temporary network sites.

In this study, calibrated and validated ground measurements from the 40 temporal sites were used to build the model for soil moisture retrieval with remote sensing datasets; ground measurements from the 15 permanent sites were used for validation.

3. Methodology

Figure 2 shows the flowchart of the procedure for SSM retrieval by fusing Landsat 8 and MODIS measurements. Landsat 8 TIR2 were fused with MODIS band 32; Landsat 8 band 4 was fused with MODIS band 1; and Landsat 8 band 5 was fused with MODIS band 2. The corresponding solar reflective and thermal emissive channels from Landsat 8 and MODIS measurements were fused first to get daily remote sensing datasets at 120 m resolution to calculate LST and NDVI, which were used in the universal triangle method for SSM retrieval. The method in this study mainly contains three parts: fusion, LST retrieval, and SSM retrieval. The fusion method is contained in the LST retrieval part.

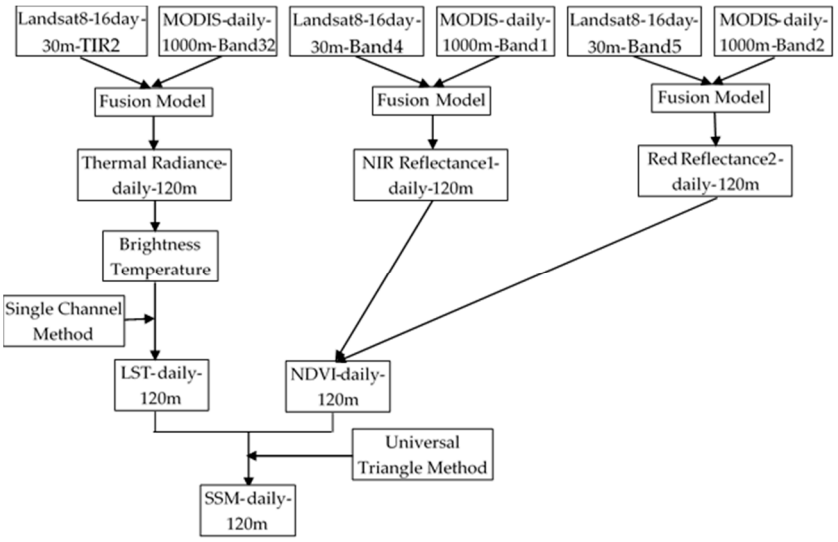

Figure 2. The flow chart for fusing MODIS and Landsat 8 measurements for surface soil moisture (SSM) retrieval.

3.1. Data Fusion

The data fusion process includes two parts: (a) generating an improved fusion method for both reflectance and radiance bands; and (b) using the LST retrieval method for the LST monitor, generating the NDVI.

We proposed an improved data fusion method based on the following assumptions: (1) the corresponding channels (solar reflective and thermal emissive channels) of Landsat and MODIS are highly consistent, and (2) the study area is homogeneous. The area of this study is a crop-covered area, and can roughly be considered a homogeneous area. For homogenous pixels, remotely sensed TIR data from different sensors at a close acquisition time should be comparable and correlated after radiometric calibration, geometric rectification, and atmospheric correction. In this study, the difference between the acquisition time of Landsat 8 and MODIS is less than 10 min, so we can consider the measurements to be acquired at the same time. However, there are still other factors such as orbit parameters, geolocation errors, effective pixel coverage, and spectral response functions, which can introduce some system biases into the subsequent analysis [17]. MODIS L1B data were resampled

to the 120-m spatial resolution with a MODIS Swath Tool (MRTSwath) provided by NASA, and the data of Landsat 8 were resampled to the same spatial resolution by applying a linear interpolation in both cases. The fusion procedure is described as follows: daily MODIS data was fused with the nearest 16-day Landsat data. For convenience, the MODIS pixel will be identified as M pixel, and the Landsat pixel will be identified as L pixel. The relationship of the radiance/reflectance between the corresponding Landsat and MODIS channels can be expressed by the following equations:

$$L(x, y, t) = m * M(x, y, t) + n \tag{1}$$

$$L(x, y, t_0) = m * M(x, y, t_0) + n \tag{2}$$

$$L(x, y, t_p) = m * M(x, y, t_p) + n \tag{3}$$

$$L(x, y, t_p) = L(x, y, t_0) + m * [M(x, y, t_p) - M(x, y, t_0)] \tag{4}$$

where L is the at-sensor radiance/reflectance of Landsat, M is the at-sensor radiance/reflectance of MODIS; and m and n are regression parameters. Then, the radiance/reflectance of the Landsat at time t_p can be generated if we know the radiance/reflectance of the MODIS at time t_0 and t_p, and the radiance/reflectance of the Landsat at time t_0 [17].

The weighting function is considered in this method. We use the distance weighting function (D), and the spectral weighting function (S), to calculate the fusion weighting function (W):

$$L(x_{ws/2}, y_{ws/2}, t_k) = \sum_{i=1}^{ws} \sum_{k=1}^{ws} W_{ik}[M(x_i, y_i, t_k) + L(x_i, y_i, t_0) - M(x_i, y_i, t_0)] \tag{5}$$

With:

$$C_{ik} = S_{ik} \times D_{ik} \tag{6}$$

$$W_{ik} = \frac{\frac{1}{C_{ik}}}{\sum_{i=1}^{ws} \sum_{k=1}^{ws} \left(\frac{1}{C_{ik}}\right)} \tag{7}$$

$$\begin{cases} S_{ik} = |L(x_i, y_i, t_k) - M(x_i, y_i, t_k)| \\ D_{ik} = 1 + \frac{d_{ik}}{A} (d_{ik} = \sqrt{(x_{\frac{ws}{2}} - x_i)^2 + (y_{\frac{ws}{2}} - y_i)^2}) \end{cases} \tag{8}$$

$$\begin{cases} ws = e,\ sum\left(\left|M(x_i, y_i, t_0) - M\left(x_{\frac{ws}{2}}, y_{\frac{ws}{2}}, t_0\right)\right|\right) < a \\ ws = e + 2,\ sum\left(\left|M(x_i, y_i, t_0) - M\left(x_{\frac{ws}{2}}, y_{\frac{ws}{2}}, t_0\right)\right|\right) > a \end{cases} \tag{9}$$

where L and M have the same meaning as above, S is the spectral weight, D is the distance weight, ws is the window size, and A is a constant parameter that depends on the window size and land cover type.

The searching size of the window depends on the difference between the surrounding pixels. If the difference between the neighboring pixels is within the threshold a, the window size doesn't need to increase. Otherwise, the size needs to be increased by a factor of 2. The initial value of the window size e depends on the different band wavelengths.

The NDVI value can be calculated by the equations as follows:

$$\text{NDVI} = \frac{\rho_{NIR} - \rho_{RED}}{\rho_{NIR} + \rho_{RED}} \tag{10}$$

where ρ_{NIR} is the reflectance of the near infrared band, and ρ_{RED} is the reflectance of the red band.

A single-channel method proposed by Jimenez-Munoz et al. was used to retrieve the LST with the fused thermal infrared data. The basis of the single channel algorithm is that the radiation attenuation for atmospheric absorption is proportional to the radiance difference of simultaneous measurements at different wavelengths. The generalized single channel method only uses the total water vapor content

and the effective wavelength, and can be applied to different sensors with the same equations [24,25]. The equation is as follows:

$$T_s = \gamma\left[\varepsilon_i{}^{-1}(\Psi_1 B_i + \Psi_2) + \Psi_3\right] + \delta \tag{11}$$

With:

$$\gamma = \{\frac{C_1 B_i}{T_i{}^2}[\frac{\lambda_i{}^4}{C_2}B_i + \lambda_i{}^{-1}]\}^{-1} \tag{12}$$

$$\delta = -\gamma.B_i + T_i \tag{13}$$

$$\begin{bmatrix} \Psi_1 \\ \Psi_2 \\ \Psi_3 \end{bmatrix} = \begin{bmatrix} \eta_{1,\lambda} & \xi_{1,\lambda} & \chi_{1,\lambda} & \varphi_{1,\lambda} \\ \eta_{2,\lambda} & \xi_{2,\lambda} & \chi_{2,\lambda} & \varphi_{2,\lambda} \\ \eta_{3,\lambda} & \xi_{3,\lambda} & \chi_{3,\lambda} & \varphi_{3,\lambda} \end{bmatrix} \begin{bmatrix} w^3 \\ w^2 \\ w \\ 1 \end{bmatrix} \tag{14}$$

where $\boldsymbol{T_i}$ is the at-sensor brightness temperature, B_i is the at-sensor radiance, λ is the effective wavelength, w is the water vapor content in the atmosphere, ε_i is the land surface emissivity, and C_1 and C_2 are the calculation parameters that can be found from Landsat 8's metadata [23]. Table 3 are parameters that were used to calculated Ψ_1, Ψ_2, and Ψ_3.

Table 3. Parameters to calculate Ψ_1, Ψ_2, and Ψ_3 through Landsat 8. TIR: Thermal Infrared.

	TIR2			
Ψ_1	$\eta_{1,\lambda}$ 0.0405	$\xi_{1,\lambda}$ −0.0809	$\chi_{1,\lambda}$ 0.2919	$\varphi_{1,\lambda}$ 0.9620
Ψ_2	$\eta_{2,\lambda}$ −0.2960	$\xi_{2,\lambda}$ 0.3611	$\chi_{2,\lambda}$ −1.0257	$\varphi_{2,\lambda}$ 0.4644
Ψ_3	$\eta_{3,\lambda}$ −0.0443	$\xi_{3,\lambda}$ 0.2509	$\chi_{3,\lambda}$ 1.4573	$\varphi_{3,\lambda}$ −0.0854

3.2. Surface Soil Moisture Retrieval

The NDVI and LST have a complicated relationship with soil moisture. Carlson and Gillies described the relationship as the vegetation index/temperature (VIT) trapezoid. The analyses of data by Carlson [26] and Gillies [27] demonstrated that there is a unique relationship among soil moisture, the NDVI, and the LST for a specific study area, which was identified as the "universal triangle". The results were later confirmed by theoretical studies using a soil–vegetation–atmosphere transfer (SVAT) model, which was designed to describe the basic evaporation processes at the surface, together with the water partitioning between vegetation transpiration, drainage, surface runoff, and soil moisture variations [28].

Figure 3 represents a schematic description of the relationship that is referred to the "universal triangle" [29]. The abscissa and the ordinate are the scaled temperature and NDVI, respectively, such that:

$$T^* = \frac{T - T_0}{T_s - T_0} \tag{15}$$

$$NDVI^* = \frac{NDVI - NDVI_0}{NDVI_s - NDVI_0} \tag{16}$$

where T is the observed LST at each pixel, $NDVI$ is the observed NDVI at each pixel, and the subscripts 0 and s stand for the minimum and maximum values, respectively.

The relationship between soil moisture, $NDVI^*$, and T^* can be expressed through a regression equation, as follows:

$$SSM = \sum_{i=0}^{i=n}\sum_{j=0}^{j=n} a_{ij} NDVI^{*(i)} T^{*(j)} \tag{17}$$

where a_{ij} are regression coefficients.

Regarding a second order polynomial, the above equation can be expanded as:

$$\begin{aligned} \text{SSM} = a_{00} + a_{10}NDVI^* + a_{20}NDVI^{*2} + a_{01}T^* + a_{02}T^{*2} + a_{11}NDVI^*T^* + \\ a_{22}NDVI^{*2}T^{*2} + a_{12}NDVI^*T^{*2} + a_{21}NDVI^{*2}T^2 \end{aligned} \quad (18)$$

In this study, we combined Equations (15), (16), and (18) to retrieve SSM through the "universal triangle" algorithm in our study area using the fused LST and NDVI measurements. Parameters in the function can be calculated by combining the ground measurement with remote sensing datasets. Numerous variations have been given to this triangle technique, including the temperature–vegetation contextual approach (TVX), the surface temperature–vegetation index (T/NDVI) space, the temperature–vegetation dryness index (TVDI), the moisture index, and the VI/Trad relation [30]. Approaches based on either the surface temperature or the complimentary temperature–vegetation index are powerful, and have clear physical meaning, but have limitations in addition to those common to all optical techniques, such as shallow soil penetration and cloud contamination. The limitations may also be affected by—and are dependent on—local meteorological conditions, such as air temperature, wind speed, and so on [31].

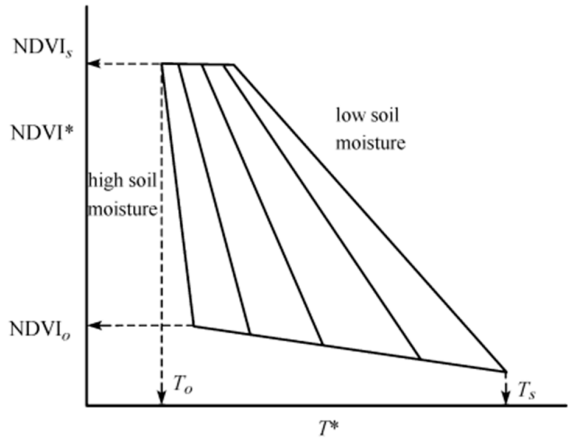

Figure 3. Universal triangle relationship between soil moisture, temperature, and the normalized difference vegetation index (NDVI) [30].

An improvement is to calculate surface soil moisture *SSM** by multiplying a function of LST, where *SSM** is the improved surface soil moisture value, and SSM is the retrieved surface soil moisture value, which can be calculated through Equations (15)–(18), where *r* and *s* are regression parameters:

$$SSM^* = SSM \times (r + \frac{s}{T^*}) \quad (19)$$

In crop-growing seasons, the NDVI will be the primary factor that indicates the living condition of plants and reveals the degree of vegetation's role in soil moisture monitoring, thus lead to the change of SSM content [32].

4. Results

Data of Landsat 8 band TIR2 were fused with MODIS band 32 measurements to get daily LST data at a high spatial resolution, and then generate LST with the single-channel method. The retrieved LST was evaluated with MODIS Land Surface Temperature product MOD11. Since there is only about a 10-min time gap between the passing time of Landsat 8 and MODIS for this study area, we can assume the remote sensing measurements were acquired at the same time, and no correction for the difference between passing time is needed. Figure 4 is a histogram showing the difference between the retrieved LST results and MODIS LST products at 120 m spatial resolution. The x-axis is the difference between

the retrieved LST and LST products in degree K, and the y-axis is the percentage of the number of pixels in each corresponding bin to the total number of pixels. Over 70% of the pixels fall in the region of the difference within 3 K. The mean error is −1.366 K, and mean relative error is −0.0045. Table 4 contains the statistics obtained from the comparison of retrieved LST against observed Landsat 8 LST.

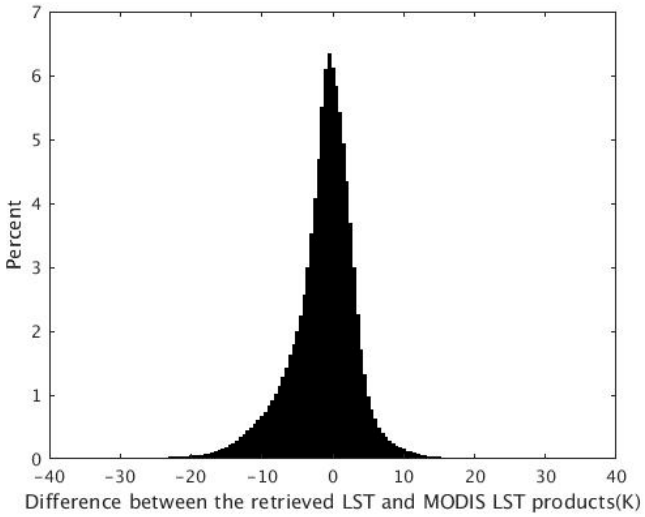

Figure 4. Histogram of the difference between retrieved land surface temperature (LST) and MODIS LST products.

Table 4. Statistics obtained from the comparison of retrieved LST against observed Landsat 8 LST.

	Mean Error (K)	Mean Relative Error	Standard Deviation of Error (K)	Standard Deviation of Relative Error
3 May 2016	−2.1255	−0.34%	3.5467	2.11%
19 May 2016	−1.2824	−0.19%	3.3550	1.86%
4 June 2016	−1.0441	−0.16%	3.2495	1.75%
20 June 2016	−1.0259	−0.16%	3.5644	2.14%
6 July 2016	−0.4340	−0.07%	2.8834	1.49%
22 July 2016	−1.3010	−0.23%	2.9697	0.56%
5 August 2016	−2.6937	−0.45%	2.2086	0.82%

To evaluate the fusion results, seven Landsat 8 passing days in the study period were selected to compare the retrieved LST and Landsat 8 LST products on the same day at 120-m spatial resolution. Figure 5 shows the scatter plots between the retrieved and LST products; we can see the distributions of the scatter plots are very close to the diagonal line, which shows that the predicted LST values are consistent with the observed ones. Absolute error and relative error were used to evaluate the method as well. The mean errors for each day ranged from −2.6937 K to −0.4340 K, and the mean relative errors for each day ranged from −0.45% to −0.07%; the standard deviation of error ranged from 2.2086 K to 3.5467 K, and the standard deviation of relative error ranged from 0.56% to 2.14%. Table 2 shows the mean error, the mean relative error, the standard deviation of error, and the standard deviation of relative error for each Landsat 8 passing day. All of these results show that the predicted LST matches the observed LST well; the fusion model has successfully retrieved the LST with a significantly improved spatial resolution (from 1000 m to 120 m), and the distribution of the different retrieved LST levels match the Landsat data well. We can see the results in May and June are not as accurate as other periods, with higher values for almost all of the mean errors, mean relative errors, standard deviation of errors, and standard deviation of relative errors; the main reason is that the land cover type changed a lot during the crop-growing seasons (from small plants to large plants). Although the whole study area can be considered a homogeneous region, the discrepancy of the land

cover condition between different study times still exists, which could lead to some errors in the retrieval method, and may result in a decrease in the accuracy of the results.

In this study, the 15 permanent sites were chosen to evaluate the predicted SSM with observed SSM. Figure 6 shows the histogram of the difference between predicted SSM and observed SSM from ground measurements; the x-axis has the unit of m^3/m^3, and the y-axis is the percentage of the number of observations in each bin. We can see that the difference ranges from -0.2 m^3/m^3 to 0.15 m^3/m^3, with a mean error of 0.034 m^3/m^3, and a mean relative error of 0.0191. Table 5 shows the mean error, the mean relative error, the standard deviation of error, and the standard deviation of the relative error for each site. The results show that this method can be applied to regional SSM monitoring with success. Figure 7 compares the SSM estimation values with the in situ SSM values for 15 sites. The x-axis is the in situ SSM values with the unit m^3/m^3; the y-axis is the retrieved SSM with the same unit. The diagonal red line in each sub-plot means that the predicted SSM is equal to the observed SSM. In general, there was a strong correlation between the SSM estimations and the in situ SSM measurements. The trends of the distribution are close to the red line, which means that the retrieved result is very close to the in situ measurements of SSM. As with LST validation, the absolute error and relative error are used to validate SSM. Overall, the values of mean error and the values of the mean relative error are quite small, which proves that this method—which aimed at improving the temporal and spatial resolution of SSM retrieval—has successfully monitored the SSM during the crop-growing season.

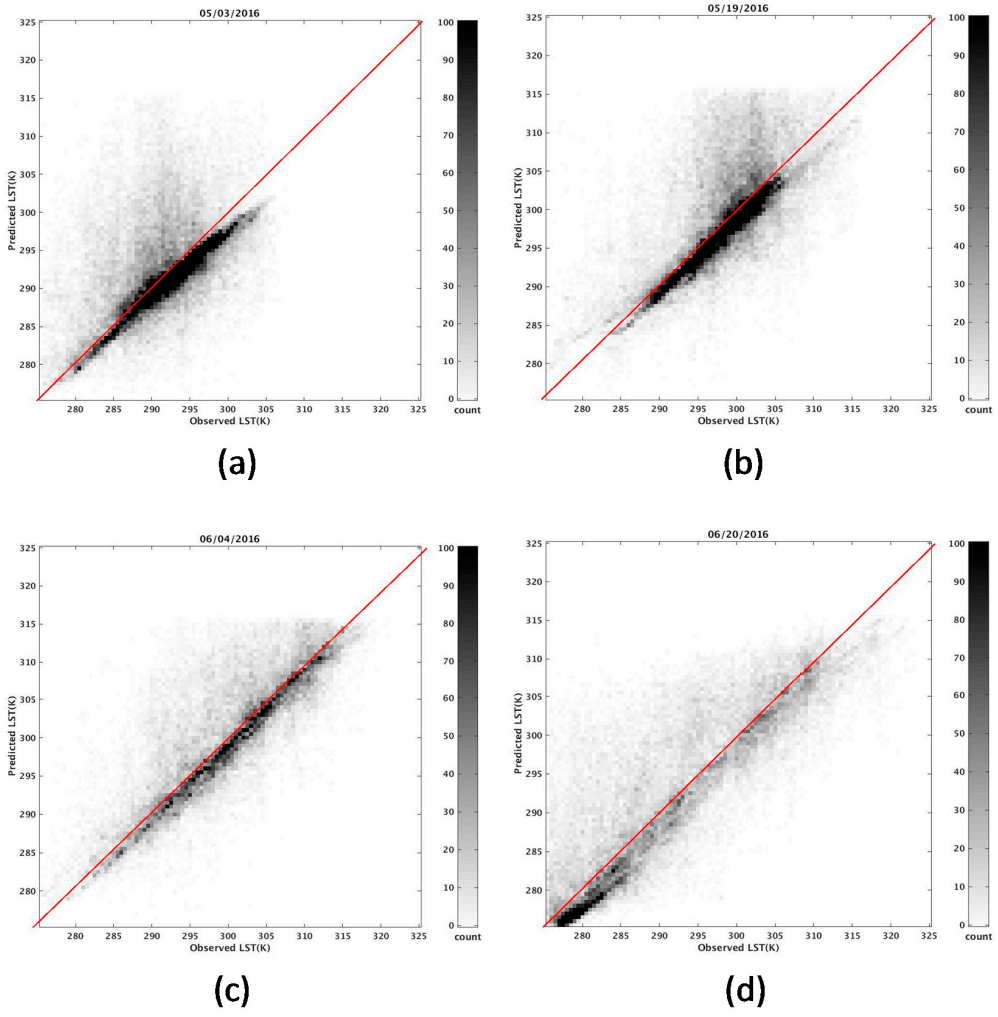

Figure 5. *Cont.*

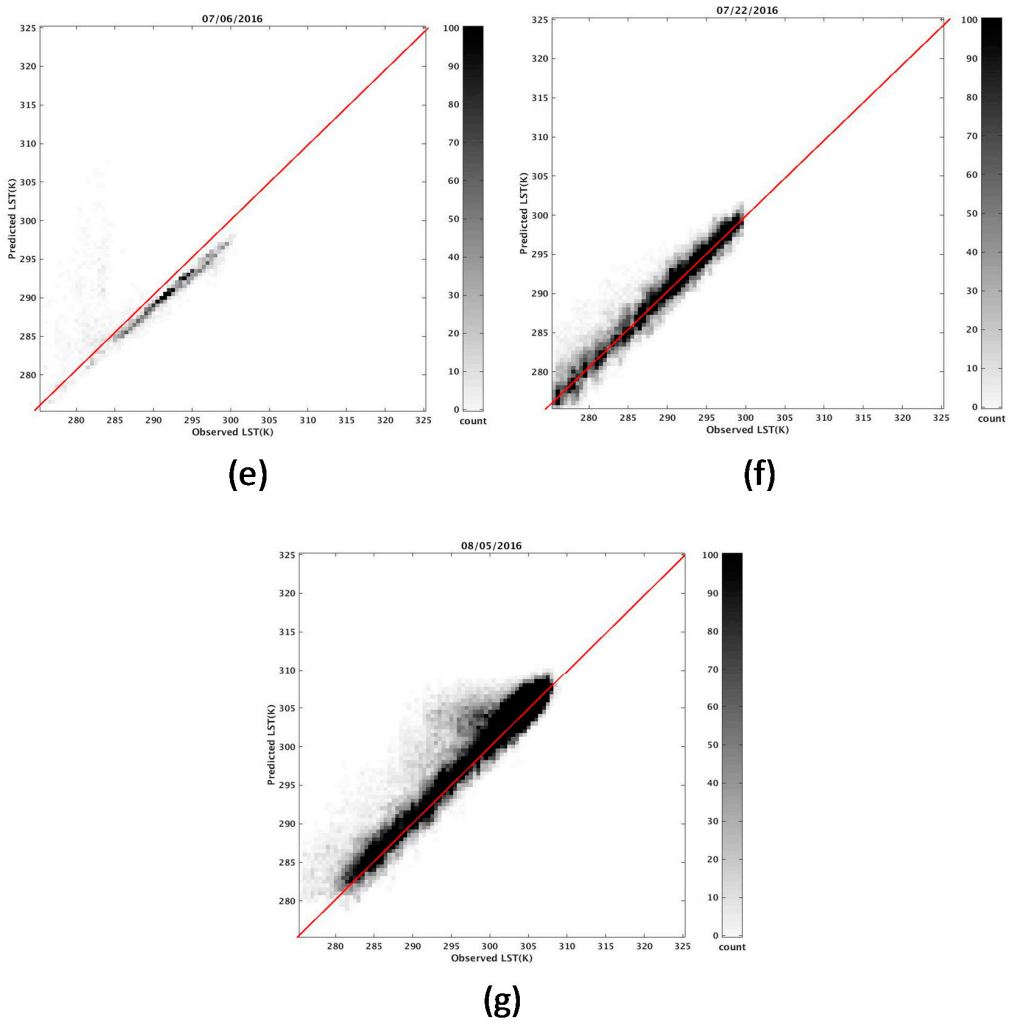

Figure 5. (**a**–**g**) represent the scatter plot between the retrieved LST and LST products at the seven Landsat passing days correspondingly.

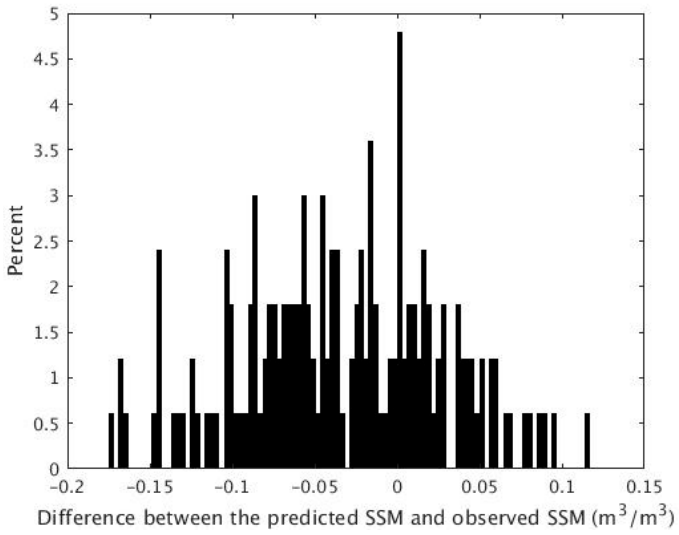

Figure 6. Histogram of the difference between predicted SSM and observed SSM.

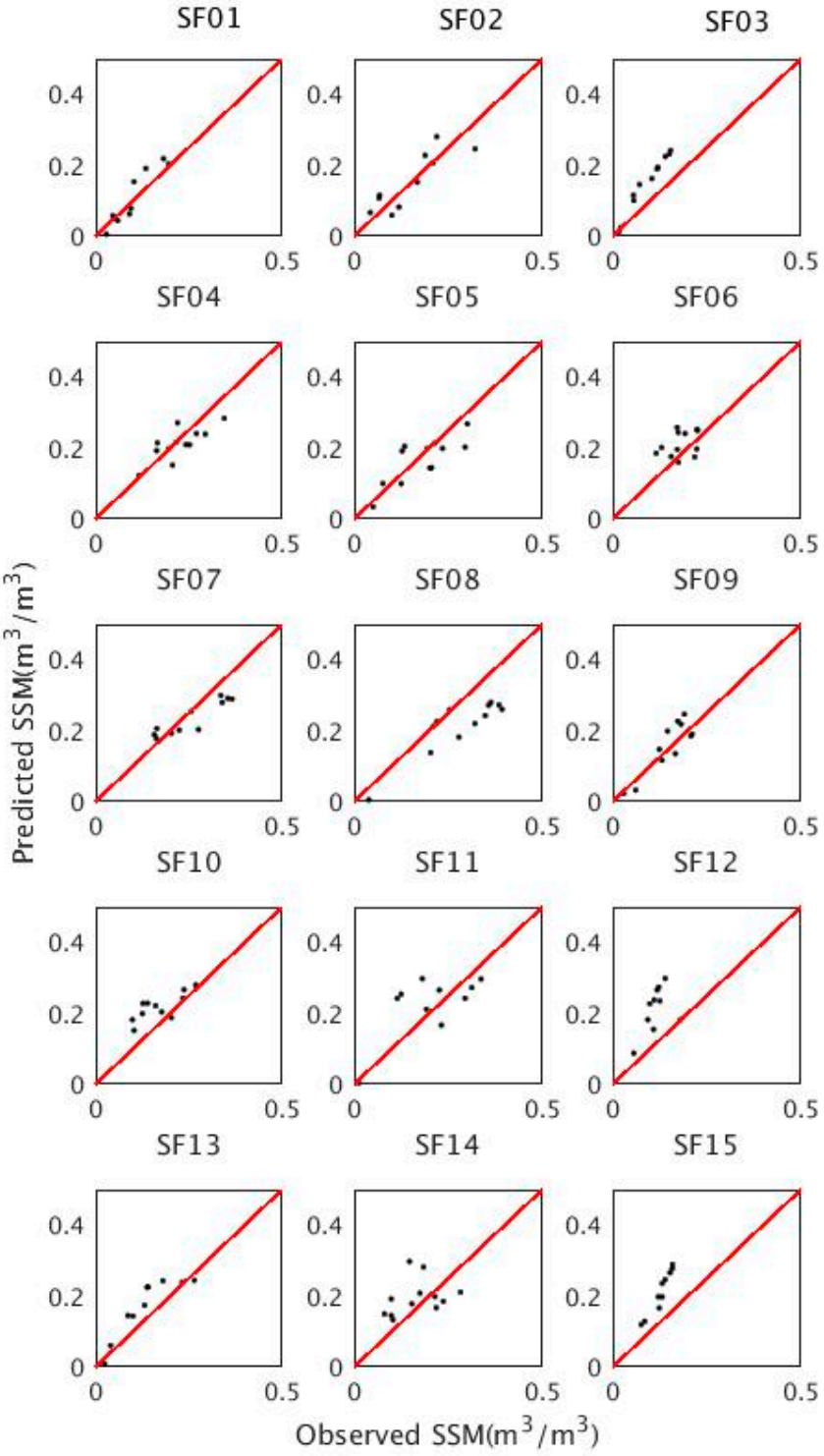

Figure 7. Results of the predicted SSM with the observed SSM.

R^2 is 0.58, and the RMSE for this study ranged from 0.0302 m^3/m^3 to 0.1124 m^3/m^3. By checking the distribution of corn and soybean fields, we found that most of the sites with relatively good retrieval results are corn sites. The main reason for this is that, during crop growing seasons, the soybean leaves contain lots of dew in the morning, which will have a big influence on the evapotranspiration circle, and flow in the soil around 7 a.m. to 8 a.m. leading to an increase of SSM. Since the in situ measurements were usually conducted between 9–11 a.m., the ground measurements of SSM were

relatively higher than the soil moisture value at the satellite passing time, which influences the retrieval model as a result. If cornfields and soybeans fields are separated, the results might be improved, but the spatial resolution in this study is not fine enough to do this. In addition, some fields have both corn and soybeans, and it would be difficult to study them separately.

Table 5. Statistics obtained from the comparison of retrieved SSM against in situ SSM measurements.

	Mean Error (m^3/m^3)	Mean Relative Error	Standard Deviation of Error (m^3/m^3)	Standard Deviation of Relative Error	RMSE (m^3/m^3)
SF01	−0.0056	0.0397	0.0238	0.1174	0.0302
SF02	−0.0031	-8.0776×10^{-4}	0.0018	0.1701	0.0434
SF03	−0.0427	−0.1387	0.0222	0.2392	0.0655
SF04	0.0090	0.0430	0.0224	0.1965	0.0402
SF05	0.0104	0.0888	0.0215	0.1737	0.0485
SF06	−0.0241	−0.1031	0.0206	0.1641	0.0500
SF07	0.0169	0.0595	0.0212	0.1512	0.0462
SF08	0.0532	0.1438	0.0286	0.2634	0.0817
SF09	−0.0067	0.0452	0.0269	0.2469	0.0354
SF10	−0.0349	−0.1678	0.0278	0.2463	0.0570
SF11	−0.0154	0.1118	0.0266	0.2341	0.0769
SF12	−0.0664	−0.0919	0.0311	0.2459	0.1124
SF13	−0.0249	−0.0473	0.0301	0.2366	0.0520
SF14	−0.0239	−0.1105	0.0292	0.2304	0.0715
SF15	−0.0566	−0.1585	0.0305	0.2333	0.0910

Figure 8 is the time series of observed SSM and predicted SSM for each site. For most of the validation sites in the study area, the trends of observed SSM and predicted SSM during the study period match well.

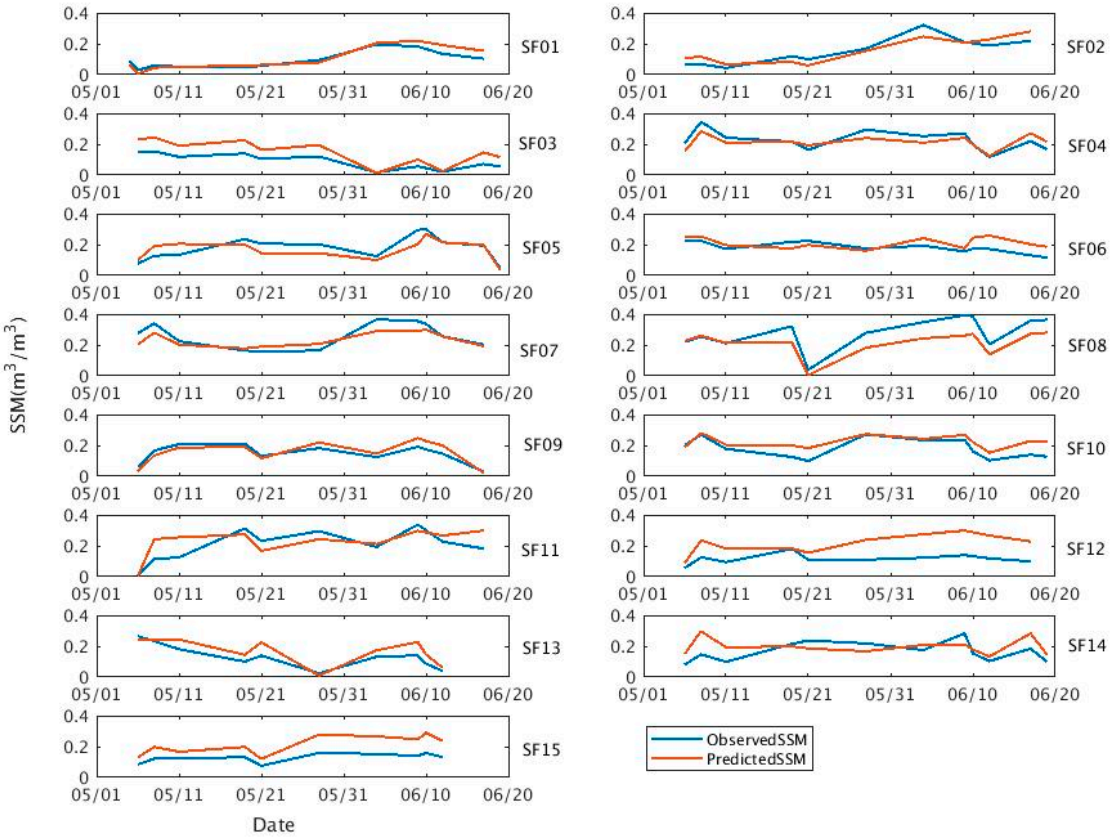

Figure 8. Time series of predicted and observed SSM.

5. Discussion

In recent years, many downscaling studies have been done for soil moisture retrieval. However, most of these works used microwave soil moisture products by combining MODIS products instead of combining Landsat and MODIS measurements. Therefore, the spatial resolution after downscaling is still over 1 km, which is not adequate enough for local applications. This study was conducted in Iowa during crop-growing seasons. The significant improvement was to combine different thermal remote sensing measurements with ground measurements for SSM monitoring at both fine spatial and temporal resolution via the universal triangle method.

The model works well for our study area, and during the study period. More datasets and studies are still needed to evaluate whether it can be applied to long-term surface soil moisture monitoring in other regions. As shown in Figure 7 and discussed above, the retrieved results show different levels of accuracy for different land cover types, which means the regression parameters in the SSM retrieval method vary a lot for the different land cover types. With the higher spatial resolution, we can distinguish different land cover types and study them separately, which may improve the accuracy of the method. In this study, we only downscaled the spatial resolution to 120 m instead of 30 m in order to ensure the appropriate accuracy of the fusion results. The spatial and temporal resolution may still be increased by adding auxiliary datasets and theories, which may significantly improve the SSM monitoring as well. Furthermore, the thermal method can still only be applied to surface soil moisture, due to the limited penetration. When considering further work on climate or agriculture issues, deeper depth soil moisture is needed, especially to include the root zone soil moisture. Combining SSM retrieval with deep depth soil moisture would be a significant and realistic achievement.

SSM is a key factor in the hydrology cycle, biochemical processes, climate change, and many other environmental issues. It also has a fundamental effect on drought and other natural hazards, which influences agriculture, water reserves, renewable energy, and the state of the ecosystem. SSM contributes to the impact on food security and human's health. The methods and results from this study can be further applied to these fields. The study of SSM monitoring offers great potential for preparedness and adaptation strategies that are of great importance to the sustainability of the economic and social sectors of society.

6. Conclusions

Landsat and MODIS are two of the most popular remote sensing sensors for SSM monitoring. However, the 1000-m spatial resolution of MODIS is too coarse to generate detailed information for a small study area. The 16-day temporal resolution of Landsat data may lead to missing valuable crop growth and development information during the growing season. Ground measurements are usually conducted in a small study area within a short period. The coarse spatial or temporal resolution makes it impossible to combine thermal remote sensing methods with ground measurements to improve the accuracy of SSM retrievals. This research proposed a downscaling method that combines the data fusion method and the universal triangle method in order to successfully retrieve daily SSM at 120-m spatial resolution. Ground measurements were used in this study to calibrate and validate the method as well. For the 15 validated sites, the mean error ranged from -0.0664 m^3/m^3 to 0.0532 m^3/m^3, the mean relative error ranged from -0.1678 to 0.1438, and the RMSE ranged from 0.0302 m^3/m^3 to 0.1124 m^3/m^3. Through some adjustments to the existing STARFM reflectance fusion model, this study successfully generated the daily LST at 120 m. For the selected days, evaluated by LST products, the mean error between the LST product and the retrieved LST is -1.3663 K, and the mean relative error between the LST product and the retrieved LST is -0.0045. The fused LST and NDVI were used for further SSM monitoring in this study; they may also be applied to other hydrology and agriculture research.

The main contributions of this paper are as follows: (1) Overcoming the unrealistic use of ground measurements to calibrate and validate the SSM model due to Landsat 8's long revisit cycle and MODIS's coarse spatial resolution in a small region by merging similar Landsat 8 and MODIS bands.

Monitoring downscale SSM through a cross-sensor method, and applying the fused measurements to regional SSM retrieval worked quite well; (2) Modifying the existing MODIS/Landsat fusion model STARFM by adjusting the search size of the window according to the value of surrounding pixels. The adjusted fusion method improved a finer resolution for both solar reflective and thermal emissive bands in the relatively homogeneous study area, and the fused channels worked well for LST and NDVI calculations; (3) Verifying the universal triangle method as an effective way of monitoring surface soil moisture for agricultural areas, especially for homogeneous land cover types. Some adjustments may be needed to improve the final results, since the effects of LST or NDVI on the retrieved surface soil moisture highly depend on other conditions. By fusing the MODIS and Landsat thermal and reflectance values, LST can be retrieved at 120-m spatial resolution with daily temporal resolution. The surface soil moisture can be retrieved through the universal triangle method at both fine spatial and temporal resolution. Through this method, another thermal remote sensing measurement may be fused as well, according to the different spatial and temporal scales needed.

Acknowledgments: This study was funded by the USGS Biologic Carbon Sequestration Program entitled "Establish a soil moisture monitoring and forecasting demonstration system by integrating satellite remote sensing measurements, in situ observations and model simulations" and by NASA/USDA entitled "Soil Moisture Active Passive Validation Experiment 2016-Iowa (SMAPVEX16-IA)". We thank Raymond R. Motha for English editing. We also thank the editors and reviewers for their valuable comments to improve this manuscript.

Author Contributions: Michael H. Cosh and John H. Prueger designed the field experiment; Michael H. Cosh and John H. Prueger contribute the in situ observation; Chenyang Xu and Xianjun Hao designed the experiments and analyzed the data; Chenyang Xu wrote the paper; John J. Qu, Xianjun Hao, Zhiliang Zhu and Laurel Gutenberg improved the manuscript.

Conflicts of Interest: The authors declare no conflict of interest.

References

1. Engman, E.T. Soil moisture needs in earth sciences. In Proceedings of the Geoscience and Remote Sensing Symposium (IGARSS'92), Houston, TX, USA, 26–29 May 1992.
2. Petropoulos, G.P.; Ireland, G.; Barrett, B. Surface soil moisture retrievals from remote sensing: Current status, products & future trends. *Phys. Chem. Earth Parts A B C* **2015**, *84*, 36–56.
3. Seneviratne, S.I.; Corti, T.; Davin, E.L.; Hirschi, M.; Jaeger, E.B.; Lehner, I.; Orlowsky, B.; Teuling, A.J. Investigating soil moisture–climate interactions in a changing climate: A review. *Earth-Sci. Rev.* **2010**, *99*, 125–161. [CrossRef]
4. Fennessy, M.J.; Shukla, J. Impact of initial soil wetness on seasonal atmospheric prediction. *J. Clim.* **1999**, *12*, 3167–3180. [CrossRef]
5. Petropoulos, G.P.; Griffiths, H.M.; Tarantola, S. A sensitivity analysis of the SimSphere SVAT model in the context of EO-based operational products development. *Environ. Model. Softw.* **2013**, *49*, 166–179. [CrossRef]
6. Vereecken, H.; Huisman, J.A.; Pachepsky, Y.; Montzka, C.; van der Kruk, J.; Bogena, H.; Weihermüller, L.; Herbst, M.; Martinez, G.; Vanderborght, J. On the spatio-temporal dynamics of soil moisture at the field scale. *J. Hydrol.* **2014**, *516*, 76–96. [CrossRef]
7. Zhang, D.; Tang, R.; Zhao, W.; Tang, B.; Wu, H.; Shao, K.; Li, Z. Surface soil water content estimation from thermal remote sensing based on the temporal variation of land surface temperature. *Remote Sens.* **2014**, *6*, 3170–3187. [CrossRef]
8. Koster, R.D.; Guo, Z.; Dirmeyer, P.A.; Yang, R.; Mitchell, K.; Puma, M.J. On the nature of soil moisture in land surface models. *J. Clim.* **2009**, *22*, 4322–4335. [CrossRef]
9. Tuttle, S.E.; Salvucci, G.D. A new approach for validating satellite estimates of soil moisture using large-scale precipitation: Comparing AMSR-E products. *Remote Sens. Environ.* **2014**, *142*, 207–222. [CrossRef]
10. Zhao, W.; Li, Z.-L. Sensitivity study of soil moisture on the temporal evolution of surface temperature over bare surfaces. *Int. J. Remote Sens.* **2013**, *34*, 3314–3331. [CrossRef]
11. Betts, A.K.; Hall, J.H.; Beljaars, A.C.M.; Miller, M.J.; Viterbo, P.A. Coupling between land-surface boundary-layer parameterizations and rainfall on local and regional scales: Lessons from the wet summer of 1993. In Proceedings of the Fifth Conference on Global Change Studies, Nashville, TN, USA, 23–28 January 1994; American Meteorological Society: Boston, MA, USA, 1994; Volume 174718.

12. Robinson, D.A.; Campbell, C.S.; Hopmans, J.W.; Hornbuckle, B.K.; Jones, S.B.; Knight, R.; Ogden, F.; Selker, J.; Wendroth, O. Soil moisture measurement for ecological and hydrological watershed-scale observatories: A review. *Vadose Zone J.* **2008**, *7*, 358–389. [CrossRef]
13. Kerr, Y.H.; Waldteufel, P.; Wigneron, J.-P.; Martinuzzi, J.; Font, J.; Berger, M. Soil moisture retrieval from space: The Soil Moisture and Ocean Salinity (SMOS) mission. *IEEE Trans. Geosci. Remote Sens.* **2001**, *39*, 1729–1735. [CrossRef]
14. Entekhabi, D.; Njoku, N.; O'Neill, P.; Spencer, M.; Jackson, T.; Entin, J.; Im, E.; Kellogg, K. The soil moisture active passive (SMAP) mission. *Proc. IEEE* **2010**, *98*, 704–716. [CrossRef]
15. Sandholt, I.; Rasmussen, K.; Andersen, J. A simple interpretation of the surface temperature/vegetation index space for assessment of surface moisture status. *Remote Sens. Environ.* **2002**, *79*, 213–224. [CrossRef]
16. Sun, L.; Sun, R.; Li, X.; Liang, S.; Zhang, R. Monitoring surface soil moisture status based on remotely sensed surface temperature and vegetation index information. *Agric. For. Meteorol.* **2012**, *166*, 175–187. [CrossRef]
17. Gao, F.; Masek, J.; Schwaller, M.; Hall, F. On the blending of the Landsat and MODIS surface reflectance: Predicting daily Landsat surface reflectance. *IEEE Trans. Geosci. Remote Sens.* **2006**, *44*, 2207–2218.
18. Weng, Q.; Fu, P.; Gao, F. Generating daily land surface temperature at Landsat resolution by fusing Landsat and MODIS data. *Remote Sens. Environ.* **2014**, *145*, 55–67. [CrossRef]
19. Hazaymeh, K.; Hassan, Q.K. Fusion of MODIS and Landsat-8 surface temperature images: A new approach. *PLoS ONE* **2015**, *10*, e0117755. [CrossRef] [PubMed]
20. Huang, B.; Wang, J.; Song, H.; Fu, D.; Wong, K. Generating high spatiotemporal resolution land surface temperature for urban heat island monitoring. *IEEE Geosci. Remote Sens. Lett.* **2013**, *10*, 1011–1015. [CrossRef]
21. Liu, H.; Weng, Q. Enhancing temporal resolution of satellite imagery for public health studies: A case study of West Nile Virus outbreak in Los Angeles in 2007. *Remote Sens. Environ.* **2012**, *117*, 57–71. [CrossRef]
22. Shen, H.; Wu, P.; Liu, Y.; Ai, T.; Wang, Y.; Liu, X. A spatial and temporal reflectance fusion model considering sensor observation differences. *Int. J. Remote Sens.* **2013**, *34*, 4367–4383. [CrossRef]
23. Zhang, W.; Ainong, L.; Huaan, J.; Jinhu, B.; Zhengjian, Z.; Guangbin, L.; Zhihao, Q.; Chengquan, H. An enhanced spatial and temporal data fusion model for fusing Landsat and MODIS surface reflectance to generate high temporal Landsat-like data. *Remote Sens.* **2013**, *5*, 5346–5368. [CrossRef]
24. Jiménez-Muñoz, J.C.; Sobrino, J.A. A generalized single-channel method for retrieving land surface temperature from remote sensing data. *J. Geophys. Res. Atmos.* **2003**, *108*. [CrossRef]
25. Jiménez-Muñoz, J.C.; Cristóbal, J.A.; Sòria, G.; Ninyerola, M.; Pons, X. Revision of the single-channel algorithm for land surface temperature retrieval from Landsat thermal-infrared data. *IEEE Trans. Geosci. Remote Sens.* **2009**, *47*, 339–349. [CrossRef]
26. Yu, X.; Guo, X.; Wu, Z. Land surface temperature retrieval from Landsat 8 TIRS—Comparison between radiative transfer equation-based method, split window algorithm and single channel method. *Remote Sens.* **2014**, *6*, 9829–9852. [CrossRef]
27. Carlson, T.N. Regional-scale estimates of surface moisture availability and thermal inertia using remote thermal measurements. *Remote Sens. Rev.* **1986**, *1*, 197–247. [CrossRef]
28. Gillies, R.R.; Carlson, T.N. Thermal remote sensing of surface soil water content with partial vegetation cover for incorporation into climate models. *J. Appl. Meteorol.* **1995**, *34*, 745–756. [CrossRef]
29. Wang, L.; Qu, J.J. Satellite remote sensing applications for surface soil moisture monitoring: A review. *Front. Earth Sci. China* **2009**, *3*, 237–247. [CrossRef]
30. Chauhan, N.S.; Miller, S.; Ardanuy, P. Spaceborne soil moisture estimation at high resolution: A microwave-optical/IR synergistic approach. *Int. J. Remote Sens.* **2003**, *24*, 4599–4622. [CrossRef]
31. Wang, L.; Qu, J.J.; Zhang, S.; Hao, X.; Dasgupta, S. Soil moisture estimation using MODIS and ground measurements in eastern China. *Int. J. Remote Sens.* **2007**, *28*, 1413–1418. [CrossRef]
32. Karnieli, A.; Agam, N.; Pinker, R.T.; Anderson, M.; Imhoff, M.L.; Gutman, G.G.; Panov, N.; Goldberg, A. Use of NDVI and land surface temperature for drought assessment: Merits and limitations. *J. Clim.* **2010**, *23*, 618–633. [CrossRef]

© 2018 by the authors. Licensee MDPI, Basel, Switzerland. This article is an open access article distributed under the terms and conditions of the Creative Commons Attribution (CC BY) license (http://creativecommons.org/licenses/by/4.0/).